


Water Body Extraction Using a Sentinel-1 Scene and Artificial Neural Networks: Case Study – Carpina-PE Dam

Juarez Antônio da Silva Júnior¹ 

Ubiratan Joaquim da Silva Junior² 

Keywords

Deep Learning
Remote Sensing
Synthetic Aperture Radar
Water resources

Abstract

Surface water is the most important resource and environmental factor for maintaining human survival and ecosystem stability, therefore accurate and timely information on surface water is urgently needed. In this study, an image classification approach using Artificial Neural Networks was proposed for mapping the surface water extent of the Carpina-PE Dam using radar image from the Sentinel-1 satellite, as well as its polarizations (VH and VV) and the generated water indices (SDWI and SWI). All datasets presented limitations in detecting small water bodies, such as narrow rivers, and overestimation in pasture areas, generating commission errors ranging from 16.5% to 28.9% and omission errors ranging from 1.47% and 3.5%, with emphasis on VH and VV polarizations. The overall classification accuracy ranged from 96% to 98% and R^2 values reached close to 1, where the best performance was seen for SDWI and SWI. The comparative experiments indicated that unitary radar polarizations with water spectral indices were useful for improving the accuracy of extracting water bodies in places with clouds, without significant variations, in addition to providing detailed information, with potential for continuous monitoring.

¹ Universidade Federal de Pernambuco - UFPE, Recife, PE, Brazil. juarez.silvajunior@ufpe.br

² Universidade Federal de Pernambuco - UFPE, Recife, PE, Brazil. ubiratan.joaquim@ufpe.br

INTRODUCTION

Surface water bodies, such as rivers, lakes and reservoirs, play important roles in socioeconomic development and ecosystem balance, and provide irreplaceable natural resources for human survival and development. Under the influence of climate change and human activities, the spatial distribution and inherent biochemical components of surface water bodies are undergoing major changes. Timely monitoring of the dynamics of surface water bodies is therefore of great importance for water-related studies and planning activities such as water resources management, prevention of water disasters and protection of aquatic environments (Zhang *et al.*, 2019; Guo *et al.*, 2022).

Recently, remote sensing data has been widely used for water mapping. Synthetic Aperture Radar (SAR), as an active microwave sensor, is not affected by cloud cover, so it acquires images at night, allows imaging in any weather, and has a wide range of observations. Therefore, mapping water bodies based on SAR images has attracted many scholars recently. Furthermore, the effective and relatively low-cost use of remote sensing to monitor floods and droughts can make a major contribution to decision-making and rescue actions (Bao *et al.*, 2021). Current methods for extracting information about water include threshold methods such as Machine Learning, Deep Learning, among others (Guo *et al.*, 2022; Li *et al.*, 2021; Rajendiran; Kumar, 2022).

Deep learning is a popular method in image processing that has been widely used in recent years (Nasir *et al.*, 2023). Artificial Neural Networks (ANNs) have been used in image classification and semantic segmentation and object detection are also used (Tamiru; Dinka,

2021; Pinheiro, 2023; Guo *et al.*, 2022). The advantage of ANNs is to capture the raw image features by multiple neural networks, which can avoid complex feature processing. ANNs for semantic segmentation are capable of performing image classification at the pixel level, which is important for extracting information from images. In ANNs, shallow artificial layers are capable of capturing pixel position information and deep artificial layers are used to label pixels. In this way, ANNs are gradually being applied to extract information about water in images (Xie *et al.*, 2023).

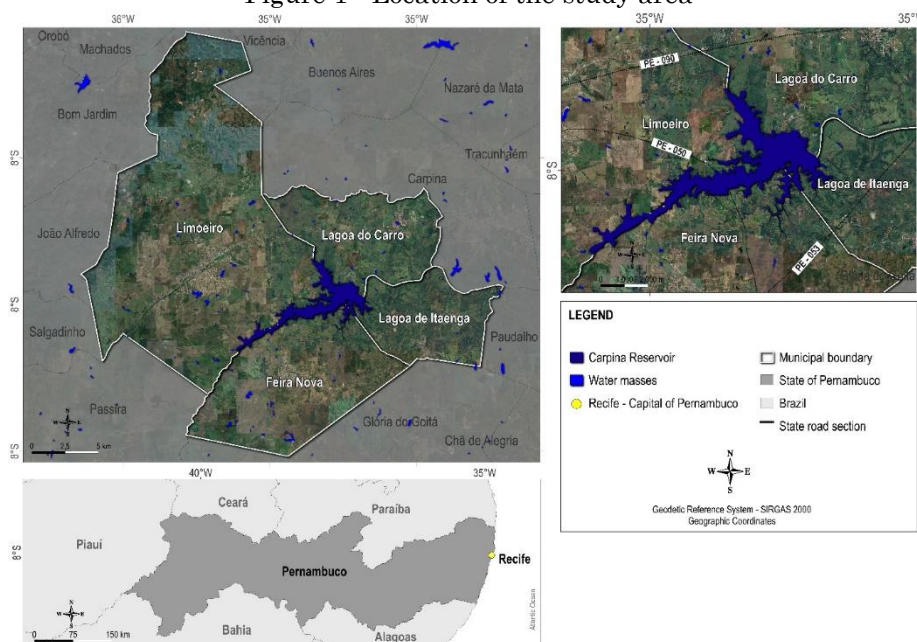
The objectives of this work are, therefore, (1) Carry out data training for image classification using the Artificial Neural Networks method, based on the number of epochs; (2) Use ANN methods to spatially extract the water body of the Carpina Dam; and finally, (3) quantitatively evaluate the performance of these algorithms, using three accuracy metrics and visual comparison.

MATERIALS AND METHODS

Study area

The Carpina dam has the following central coordinates: 7°53'28"S 35°21'45"W. It is located between the municipalities of Limoeiro, Lagoa do Carro, Lagoa de Itaenga and Feira Nova, and has a storage capacity of 270 million cubic meters of water. The dam is currently used for public water supply, fish farming and flood control in the Recife Metropolitan Region (RMR). Its main function is to control floods on the Capibaribe River. It was built by the extinct Departamento Nacional de Obras e Saneamento (DNOS) in 1978, in response to the major flood on the coast of Recife in 1975 (Lambert, 2021).

Figure 1 - Location of the study area



Source: The authors (2023).

The Carpina Dam is one of the largest water dams in the state of Pernambuco and one of the most important in the Capibaribe River hydrographic basin, and plays an important role in containing floods, also being used as a supplier of water for human consumption to from the year 2002 (Costa Júnior, 2022).

Sentinel-1 data and preprocessing

Sentinel-1 is a synthetic aperture radar program, which has a constellation of two polar-orbiting satellites (Sentinel-1A and Sentinel-1B). A set of Sentinel-1A images (track 69) was used in this study for the detection of the Carpina Dam. The images were obtained from the European Space Agency (ESA), through the Copernicus (2023), referring to August 20, 2022. The S1A_IW_GRD Level-1 products used correspond to the wavelength of 5.6 cm in VV and VH polarizations, operating in the C band (5.405 GHz). The images obtained have a bandwidth of approximately 250 km and a spatial resolution of 10 m, where each pixel contains radar backscatter intensity values (Son et al., 2021).

The Science Toolbox Exploitation Platform (SNAP) toolset developed by the European Space Agency (ESA) was used for preprocessing SAR data, with the Graph Processing Tools (GPT) of ESA's Toolbox (S1TBX). These steps include Radiometric Calibration, Speckle Filter and Terrain Correction. The purpose of SAR calibration is to provide images in which pixel values can be directly related to radar

backscatter. In this way, the radiometric calibration converts the raw pixel signals of the S1A_IW_GRD products on the digital number scale (ND), into zero sigma backscatter intensities (σ^0). Due to the coherent interference that appears in SAR images, due to the different elementary scatterings of the reflected electromagnetic waves, a disturbing phenomenon known as speckle occurs. This phenomenon introduces noise into the pixel intensities of the image, resulting in variations that exhibit a granular pattern and compromise the ability to interpret the image appropriately.

To reduce speckle noise, speckle filtering was used with a Lee filter, with a window size of 3x3 pixels. Minimizing noise is essential for better information extraction in this type of image. Subsequently, Range Doppler Terrain Correction was applied to geocode the images, since the geometry of the SAR system's side view and the Earth's topography cause several distortions. This correction was made using the Shuttle Radar Topography Mission (SRTM) (Filipponi, 2019).

Dual-Polarized Water Index (SDWI)

The selection of a water index is of crucial importance for the extraction of water bodies by remote sensing. In this work, in addition to VV and VH polarizations, the water body was also extracted using the Sentinel-1 Dual-Polarized Water Index (SDWI) (Nasir et al., 2023). Dedicated to Sentinel-1's dual-polarized bands, this index can effectively distinguish the

difference between water and other objects in dual-polarized wavebands, and can enhance information from surface water bodies and eliminate disturbances from other surface types such as vegetation and soil. The SDWI is calculated using the VH and VV images calibrated through equation 1.

$$SDWI = \ln 10 * VV * VH - 8 \quad (1)$$

Where VV and VH denote the pixel values of the median image VV and median image VH, respectively.

SAR Water Index (SWI)

The SWI (SAR Water index) is a useful index for delimiting water bodies and monitoring droughts obtained from Sentinel-1's calibrated VH and VV polarizations. The SWI was constructed based on the linear regression equation between Sentinel-1 and MNDWI (The Modified Water Normalized Difference Index) data from Sentinel-2 (Tian *et al.*, 2012). At the same time, SWI has a similar characteristic to MNDWI, based on Equation 2:

$$SWI = 0.1747 \times VV + 0.0082 \times VH \times VV + 0.0023 \times VV^2 - 0.0015 \times VH^2 + 0.1904 \quad (2)$$

Training and Classification by Artificial Neural Networks

Artificial Neural Networks (ANN) are a form of artificial intelligence that simulates some functions of the human brain to associate the correct Water and non-Water classes with image pixels, in this case, the VH, VV, SWI and SDWI images. ANN-based classification uses a non-parametric approach and therefore it is accessible to incorporate supplementary data into the classification process to improve accuracy. An ANN consists of a series of layers, each containing a set of processing units called neurons. All neurons in a given layer are linked by weighted connections to all neurons in previous and subsequent layers. During the training phase, the ANN learns about the regularities present in the training data and then builds rules that can be extended to unknown data (Giles *et al.*, 2021).

The training dataset was used to update the network parameters during each cycle (hereafter referred to as an epoch), where the network outputs are compared with the training data and the loss is calculated based on their differences. Network parameters were adjusted to minimize error. The number of epochs refers

to the number of times the entire training data set is passed back and forth through the neural network. Each epoch consists of a forward pass, where the input data is processed by the network to obtain output predictions, followed by a reverse pass, where the network parameters (weights and biases) are adjusted based on the calculated errors (Salah, 2017).

The validation set tests the network at the end of each epoch and is used to vary the hyperparameters associated with training, such as the learning rate, as well as determine when the network has completed training (Hasan *et al.*, 2019). The test dataset was later used to evaluate the accuracy of the fully trained network, so that approximately 70% of the data was used for training and 30% for validation. The network was trained on thirty epochs of the entire dataset.

Reference data and accuracy analysis

Water body accuracy analysis was considered using a pixel grid with a finer resolution reference cell size compared to the 10 m Sentinel-1 data, which allowed an assessment of body density based on accuracy assessments traditionally performed using a confusion matrix. The reference map adopted in this study was a full coverage section of the dam's water body using a PlanetScope R/G/B/NIR image, with a spatial resolution of 3 m, from the same month as the Sentinel-1 image used. This image was obtained from Planet (2023).

The validation procedures, as well as the use of PlanetScope data for this purpose, are in accordance with the international protocol of "Geospatial Data Validation Procedures and Techniques" proposed by Balakrishnan (2019), which describe the set of rules and best practices to confirm the quality of geospatial data taking into account Visual Quality Control, Data Acceptance Criteria Level, Position Accuracy, Inconsistency, Thematic Accuracy, and Attribute Verification.

Based on the elements of the confusion matrix, it was possible to generate four thematic accuracy evaluation coefficients and describe the adequacy between the generated classes and the reference data, including the Omission Errors (OE), Commission Errors (CE) and the Kappa Coefficient. The OE is the relationship between the pixel belonging to category *i* in the reference map, but which was categorized as *j* in the classified map, while the CE is when the reference indicates that the pixel belongs to the non-membership category *j*, but in the map it was classified as relevance *i*, respectively. The Kappa coefficient is a statistical method for

evaluating the level of agreement between two sets of data. The mathematical formulation of each estimate can be found in Nasir *et al.* (2023).

Figure 2 - Photographs of the surroundings of the Carpina Dam.



Source: The authors (2023).

For the analysis of geographic space, the relationship between the visual image of the researcher in the field (local scale) and the vertical image of the study area (landscape scale) often allows the so-called “terrestrial truth” to be defined, in order to validate a classification of scenes obtained by orbital sensors. To this end, measuring geographic coordinates in the landscape image is essential. However, it is common in these cases to carry out a sequence of image records, obtained by GPS instruments (Henke-Oliveira, 2022).

Aiming to integrate the data obtained at different scales and assist in the recognition of patterns in a visual way, for the selection of training samples, a field survey was carried out in the study area, on 03/22 and 03/23. The field analysis was based on the inspection of local landscape dynamics, recording photographs and obtaining coordinates using the GPS Tools application. The sample points with categorical information were inserted into the training and classification process. Due to the impossibility of movement and safety, remote and internal areas of the water body were not covered. On the other hand, the points collected made it possible to describe the natural systems surrounding the water body.

Regression by grid proportion 0.5 km x 0.5km

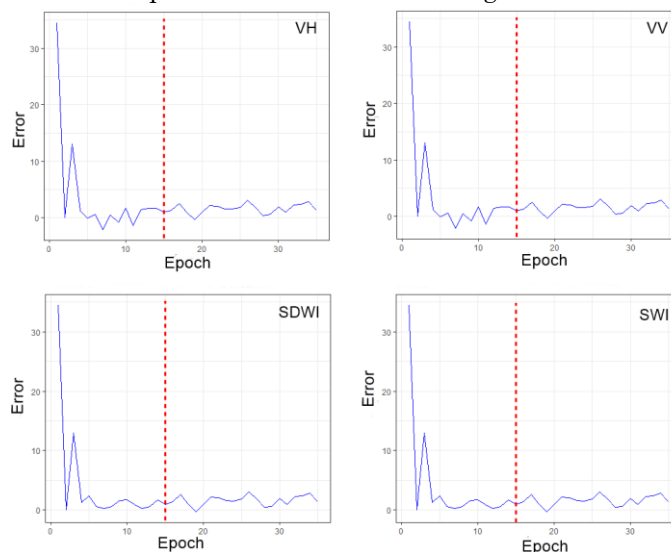
The proportions of water features classified by ANN (VH, VV, SDWI and SWI) were defined separately in cells of a 0.5 km x 0.5 km grid, as well as the validation product, for comparison by linear regression simple. The Linear Regression Coefficient of Determination (R^2) and the regression slope and intercept terms summarize the precision and accuracy of the proportions classified as Water and Non-Water, respectively (Boschetti *et al.*, 2019). If the 3 m errors of omission and commission compensate each other in the 10 m grid cells, then the R^2 and slope coefficient will be close to unity and the intercept will be close to zero, indicating high precision and accuracy of the classified Water features by area proportions.

RESULTS

Training Analysis ANN

Figure 3 shows the convergence of the Error in relation to the number of epochs for the set of sample pixels VH, VV, SDWI and SWI. As shown, the training errors are very similar to each other and have converged to the minimum and stable value possible.

Figure 3 - Relationship between Error in the image dataset using 30 epochs.



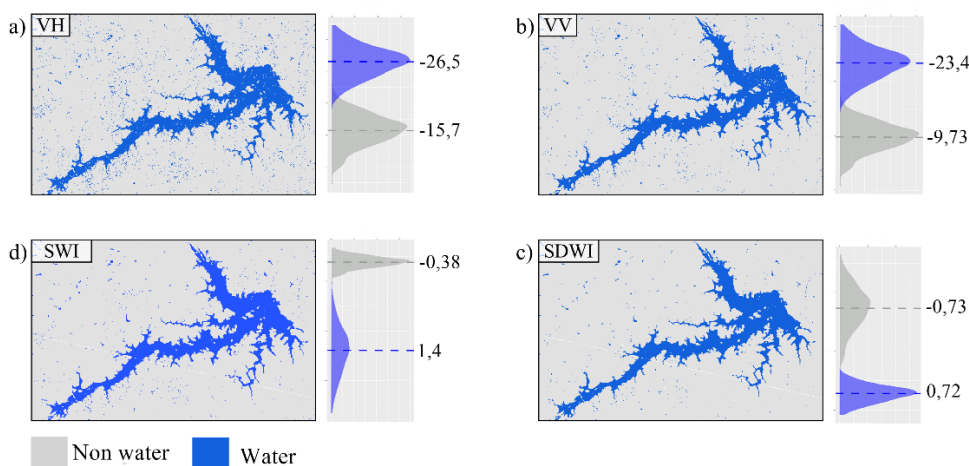
Source: The authors (2023).

Overall, adjusting the number of epochs based on validation performance can help avoid overfitting and achieve better generalization. A similar behavior is observed in the data set, where the largest error is seen in the initial training epochs, with instability in the 5° and 10° training epochs. It was also identified that the point at which the network begins to overfit or when validation accuracy stabilizes is when training reaches the 15° epoch, with error values below 5. After the 15th epoch, there was stabilization without significant variations, therefore in the ANN classification process, a number of epochs equal to 15 was used in the four classification models.

Water body extraction performance by photointerpretation

The ANN method can automatically determine the segmentation threshold based on support vectors and image histogram, which is widely used in water body extraction, in combination with SAR unit bands and water indices (*Guo et al., 2022*). In this section, the general performance of the method applied entirely in the study area was visually compared. The results of extraction from the water body using the ANN method are shown in Figure 4.

Figure 4 - Water bodies obtained by ANN for the S1 polarizations VH, VV and the water SAR indices SDWI and SWI.



Source: The authors (2023).

It can be seen visually that the delimitations of the water bodies did not present significant variations between them, that is, they all fully showed the spatial distribution of the dam's

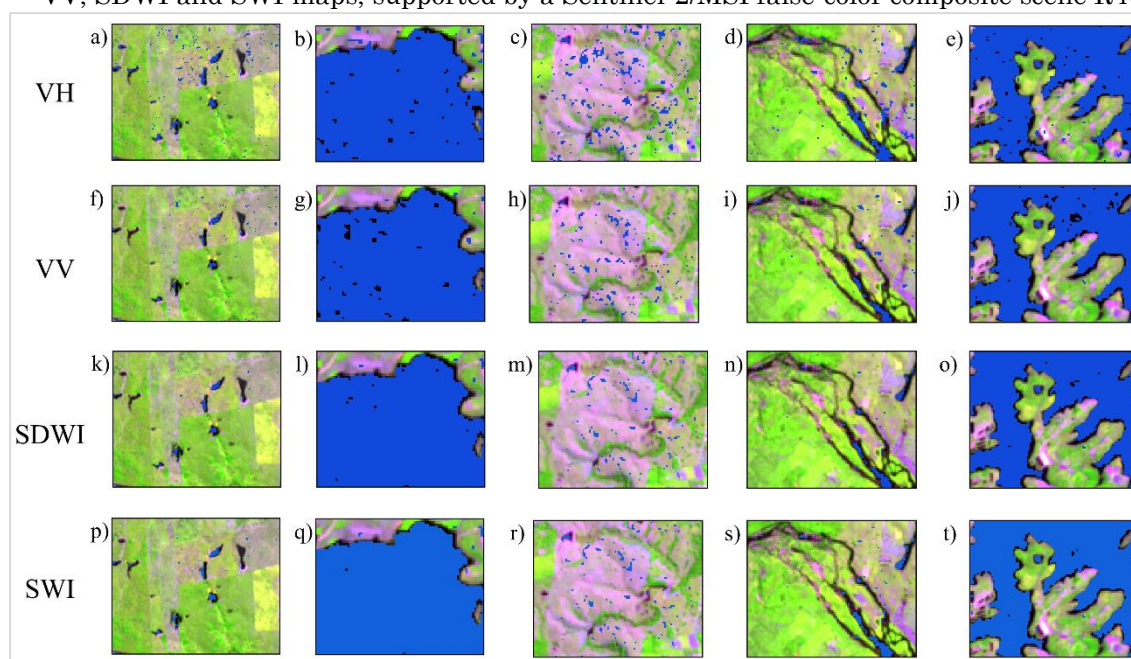
water body. Despite this, the maps showed an important variation in the detection of small lakes around the dam, with emphasis on the VH and VV maps, where the high distribution of

isolated pixels of water bodies is visible throughout the study area. The advantage of using SAR spectral indices can effectively solve the deficiency of a single polarization image and distinguish water areas. Furthermore, feature detection through ANN classifier can reduce the interference of invalid data caused by noise, thereby improving operation efficiency and classification accuracy.

The feature of unitary polarizations (VV and VH) does not necessarily improve classification

accuracy, because some features may have correlation and redundancy due to similar dispersion characteristics, resulting in a high distribution of isolated pixels without a clear relationship with water bodies. The visual comparison of the delimitation of the dam's water surface using different methods in the SAR image continued with some peculiarities shown in Figure 5.

Figure 5 - Local visualization panels for the different sectors of the Carpina Dam based on the VH, VV, SDWI and SWI maps, supported by a Sentinel-2/MSI false-color composite scene R4G8B12.



Source: The authors (2023).

The mapping of small lakes around the dam was a limiting factor and a source of errors in the quality of detection, as can be seen in figure 3, where the VH and VV polarizations detected false positives (noise) and some lakes were not completely detected on Figure 3a, b, e and j. SDWI and SWI, despite the lower presence of noise, also did not detect some bodies, in addition to having limitations in detection at the edges, failing to classify the majority of water bodies (Figure 3k and p). In the water body, located close to the dam line, the classifier showed a peculiarity in detection. The VV and VH polarizations showed some pixels without the presence of water in this sector (Figure 3b and g), while the SDWI showed a smaller distribution of “No water” pixels within the water mass (Figure 3). Similar behavior to SDWI was also seen in the SWI composite, on the other hand, the best detection was seen in

SWI, showing a set of homogeneous pixels and few gaps (Figure 3 q).

Pasture areas were also targets of poorly detected pixels in all four cases. The VV and VH polarizations were the ones that most erroneously detected water pixels in pasture features (Figure 3c and h). SDWI and SWI showed similar behavior to VV and VH, with some overestimations, while with a lower distribution of noisy pixels in these areas (Figure m and r). In Figure 3d, i, n and s it is possible to observe that none of the data sets were able to detect water pixels in narrow stretches and on the edges of the water body, showing a significant retreat, especially in figures 3e, j, o and t, probably related to pixels affected by spectral mixing, with spectral information from soil and water, where they were not considered by the classifier as a body of water.

Analysis by Commission Error, Omission and Kappa Coefficient

By calculating the elements of the binary Contingency Matrix generated through images

classified by ANN and PlanetScope data, table 1 shows the commission and omission error coefficients and Kappa, in the accuracy analysis of the detection of water bodies.

Table 1 - Omission and Commission Errors and Kappa Coefficient for the different S1 data.

	VH	VV	SDWI	SWI
OE (%)	3,5	2,9	2	1,47
CE (%)	28,9	20,3	16,5	19,3
Kappa	0,79	0,86	0,89	0,88

Source: The authors (2023).

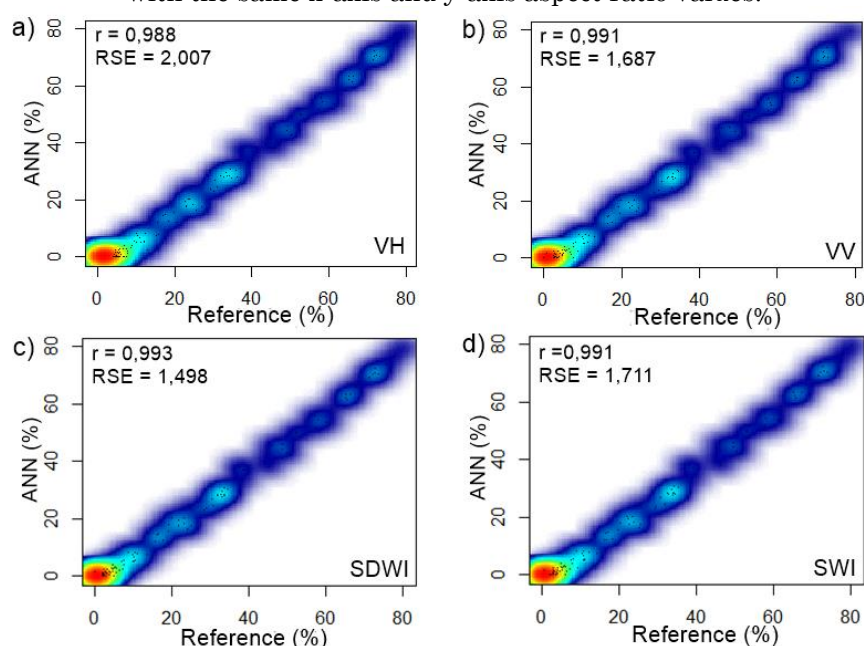
All datasets had low omission error ($OE < 4$), where SWI performed best and VH and VV polarizations had the highest error estimates. The result obtained, shown by SWI, may be strongly related to the greater spatial adherence with the reference map, reaching 91%, while VH, VV and SDWI were 81%, 84% and 89%, respectively. The VH and VV polarizations presented the highest commission error estimates, both with an overestimation of 0.28 km^2 and 0.23 km^2 while the SDWI, which presented the smallest commission error, presented 0.16 km^2 of area without its correct class assignment. "Not water" SWI presented a moderate estimate of EC, with a value close to VV polarization. Based on the Kappa coefficient values, SDWI and SWI showed better performance in relation to VH and VV unitary polarizations, although it is important to note that they all presented high Kappa coefficient

values ($Kp > 0.78$) and without significant variations ($0.79 \sim 0.89$).

Linear Regression Metrics on 0.5 km x 0.5 km grid

To complement the comparison analyzes between the ANN product (VH, VV, SDWI and SWI) and the PlanetScope reference data, based on the "Water" and "Non-Water" classes, figure 6 shows a scatterplot of the proportions of grid cells by the ANN product versus the grid proportions by the spatial reference product. Grid cells with lateral dimensions of 0.5 km were considered, as they are larger than the Sentinel-1 pixel dimension of 10 m, but small enough to minimize the occurrence of cells with similar proportions to Water features in both products.

Figure 6 - Scatter plots of the proportion of area classified as Water in cells of a 0.5 x 0.5 km grid, as defined by the ANN classification for each dataset (y-axis) and the PlanetScope reference data (x-axis), fully understood in the study area. The rainbow color scale illustrates the frequency of cells with the same x-axis and y-axis aspect ratio values.



Source: The authors (2023).

Both the precision parameters and the SDWI and SWI indices demonstrated good performance when related to the reference map, exhibiting a significant linear relationship ($R^2 \sim 0.9$). The VH and VV polarizations also revealed high estimated R^2 , with a small discrepancy between them. Although VH and VV polarizations showed a slightly larger slope, SDWI revealed the smallest linear coefficient. The SWI, in turn, exhibited an angular coefficient close to 1, suggesting a more expressive agreement with the reference image. While VH and VV exhibited linear coefficients greater than about 0.014, SWI also demonstrated a similar estimate. In a broader context, the regression analysis revealed that all datasets played a relevant role in detecting water bodies. This translated into a coefficient of determination (R^2) that exceeded 0.95, achieved with a confidence level of 95%.

DISCUSSION

In summary, the ANN architecture has proven to be a powerful and stable method for binary water classification, but there are still some factors that affect its accuracy. Limitations in the identification of some classes, such as pastures, may be a deficiency in detection, and the main cause of commission errors above 10% for all data sets, however, an increase in the number of samples and a new adjustment of ANN parameters can attenuate the distribution of noisy pixels. Pasture and clear-cutting areas have low backscatter in the four types of existing polarizations, quite similar to that found in water bodies, since part of the incident radar energy is capable of penetrating the soil surface, resulting in lower backscattered intensity (Wang *et al.*, 2013). This similarity can cause inconsistencies in the ANN architecture to separate these areas. Extraction precision is generally more susceptible to noise with properties similar to those of water, which makes it difficult to distinguish them in SAR unitary polarization images. Therefore, some of the reasons for a small error of commission and omission can be understood.

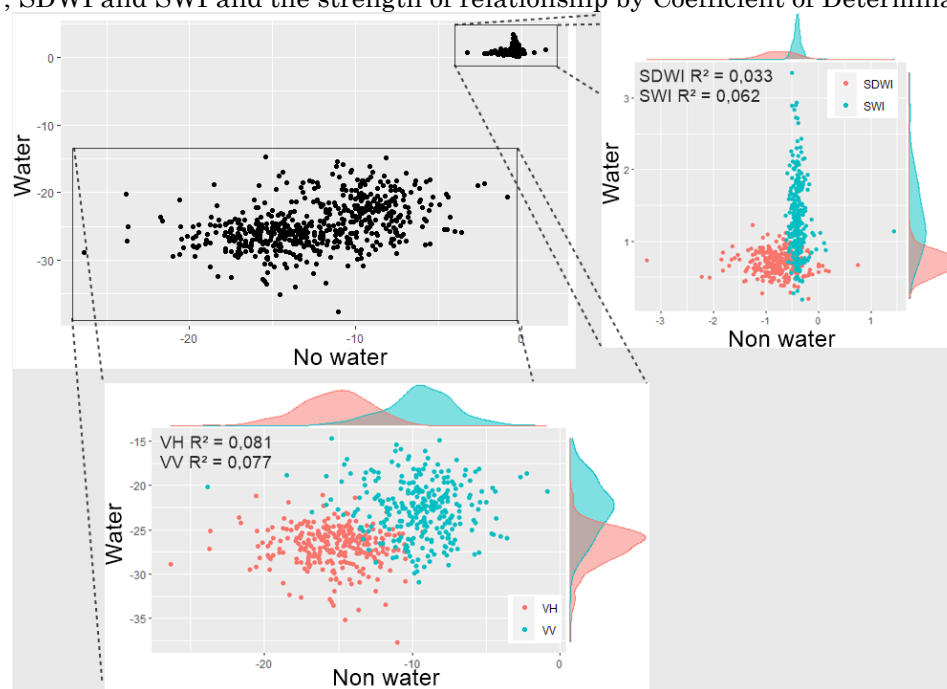
Although the SDWI and SWI indices have the ability to filter out overestimated pixels,

they cause some problems. After the SDWI and SWI indices were employed, although there were still false detections, water extraction was performed, but inevitably caused missed detections, as shown in Figure 3n and s. The results showed that the dataset based on SDWI and SWI had the highest accuracy and best water body extraction result when compared to the VH and VV unitary polarizations. The main reason is that the SDWI and SWI sets for the Water and Non-Water classes have less relationship between them, as can be seen in the lower R^2 values in Figure 6. Therefore, the ability of ANN to predict the elements of water increases, very different from the classification carried out by unique information from separate polarizations.

However, the method showed a relatively fragmented result in the extraction of small bodies of water, in addition to the extraction of narrow rivers which was poor, leading to important errors of omission. In fact, for monitoring large surface water bodies, small ponds, small reservoirs and narrow rivers can be reasonably neglected due to their low importance, as we are mainly concerned with the analysis of surface water change for the study area as one all. The fact that these features were omitted is not unexpected, since the water class, defined as a pixel with mixed spectral behavior of water and vegetation or soil reflectance, which in turn, was not included by the ANN classification. Misclassified pixels were also found in the dam's water mass, mainly in VH and VV polarizations. The reason for this may have been because the water surface is not smooth and some backscatter pixels do not show the characteristics of the water body, causing confusion in the classifier and mainly affecting the original polarizations. In this case, in the SDWI and SWI indices, these noise pixels in the water body are attenuated. Despite this, the use of Sentinel-1 images, combined with ANN, proved to be important for extracting water bodies, with omission errors below 4%, and $R^2 > 0.9$, that is, a large part of the mirrors d' water was effectively detected by the dataset.

Finally, the classification results for all tested methods (Figure 2), suggest that the proposed method can adequately capture water coverage, noting that the effect of extracting open water and small areas of water can be an important factor in detection quality.

Figure 7 - Scatterplot illustration of the distribution of “Water” and “Non-water” pixels for the sets VH, VV, SDWI and SWI and the strength of relationship by Coefficient of Determination (R^2).



Source: The authors (2023).

CONCLUSIONS

In general, the following conclusions can be mentioned:

(a) Classification of water bodies using S1 unitary polarization images (VH and VH) can cause overestimations, especially in low backscatter pixels of some types of land cover, with commission error varying between 16 and 29%.

(b) The recognition of linear water bodies and small lakes is still a challenge, since the data combinations used in this study showed limitations in detecting these areas, being capable of generating average omission errors of 2.5%.

(c) The polarimetric water indices SDWI and SWI showed, in general, the best classification performance, and the lowest correlation between the “Water” and “Non-Water” classes, providing accurate extraction, especially in locations with water bodies and smaller sensitivity of the spectral mixture found at the edge of the dam, showing a Kappa coefficient between 0.88 and 0.89.

(d) The results obtained from the exploration of Sentinel-1 data indicate that the Sentinel constellation is a powerful tool for mapping and monitoring large, complex and sensitive ecosystems, such as water reservoirs in the Brazilian Northeast, allowing a very high revisit

frequency. high. Despite this, the method has not been tested in places with shadows, rugged terrain, speckle noise and different angles of incidence, which could be objects of study for future work.

(e) The use of Artificial Neural Networks (ANNs) for training and classification demonstrated efficiency in executing the surface water mapping task, minimizing the error resulting from pre-processing. This was achieved by optimizing the number of epochs used, showing that the method was not sensitive to the complexity of the data.

Finally, the method applied in this study was relatively simple and can meet high precision requirements, which is of great importance for the practical application of water resources management through digital radar image processing methodologies.

REFERENCES

- BAO, L.; LV, X.; YAO, J. Water Extraction in SAR Images Using Features Analysis and Dual-Threshold Graph Cut Model. **Remote Sensing**, [S.l.], v. 13, n. 17, p. 3465, 2021. <http://dx.doi.org/10.3390/rs13173465>.
- BOSCHETTI, L.; ROY, D. P.; GIGLIO, L.; HUANG, H.; ZUBKOVA, M.; HUMBER, M. L. Global validation of the collection 6 MODIS

- burned area product. **Remote Sensing of Environment**, [S.l.], v. 235, p. 111490, 2019. <http://dx.doi.org/10.1016/j.rse.2019.111490>
- BALAKRISHNAN, M. **Geospatial Data Validation Procedure and Techniques. International Archive of Applied Sciences And Technology**, [S.l.], v. 10, n. 1, p. 148-153, 2019. https://soeagra.com/iaast/iaast_march2019/25f.pdf
- COPERNICUS, **Data Space Ecosystem**. (2023). Available: <https://dataspace.copernicus.eu/> Accessed on: nov. 10, 2023.
- COSTA JÚNIOR, J. **Uso do modelo digital de elevação e do modelo digital de terreno para atualização dos dados de barragens e capacidade de armazenamento de reservatórios em Pernambuco**. 2022. Trabalho de Conclusão de Curso (Engenharia Civil) – Universidade Federal de Pernambuco, Caruaru, 2022.
- FILIPPONI, Federico. Sentinel-1 GRD Preprocessing Workflow. **3Rd International Electronic Conference On Remote Sensing**, [S.l.], p. 100-115, 2019. <http://dx.doi.org/10.3390/ecrs-3-06201>
- GILES, A. B.; DAVIES, J. E.; REN, K.; KELAHER, B. A deep learning algorithm to detect and classify sun glint from high-resolution aerial imagery over shallow marine environments. **ISPRS Journal of Photogrammetry and Remote Sensing**, v. 181, n. 7, p. 20–26, 2021. Available: <https://www.sciencedirect.com/science/article/abs/pii/S0924271621002367?via%3Dihub>. Accessed on: mar. 27, 2023.
- GUO, Z.; WU, L.; HUANG, Y.; GUO, Z.; ZHAO, J.; LI, N. Water-Body Segmentation for SAR Images: past, current, and future. **Remote Sensing**, [S.L.], v. 14, n. 7, p. 1752, 2022. <http://dx.doi.org/10.3390/rs14071752>
- HASAN, M.; ULLAH, S.; KHAN, M. J.; KHURSHID, K. Comparative analysis of SVM, ann and cnn for classifying vegetation species using hyperspectral thermal infrared data. The International Archives of the Photogrammetry, **Remote Sensing and Spatial Information Sciences**, v. XLII-2/W13, n. 1, p. 1861–1868, 2019. Available: <https://www.int-arch-photogramm-remote-sens-spatial-inf-sci.net/XLII-2-W13-1861-2019/isprs-archives-XLII-2-W13-1861-2019.pdf>. Accessed on: mar. 27, 2023.
- HENKE-OLIVEIRA, C.; HIROO SAITO, C. A imagem da paisagem e a paisagem da imagem: o sistema de aquisição, processamento, hospedagem e integração de informações sobre recursos ambientais (SAPHIRA). **Revista Espaço e Geografia**, [S. l.], v. 15, n. 2, p. 385:405, 2022. Available: <https://periodicos.unb.br/index.php/espacoegografia/article/view/39947>. Accessed on: mar. 27, 2023.
- LAMBERT, M. P. **Estudo dos indicadores de risco de inundação no município do Recife decorrente do rompimento hipotético da barragem de Carpina**. 2022. Trabalho de Conclusão de Curso (Engenharia Civil) - Universidade Federal de Pernambuco, Caruaru, 2021.
- LI, M.; HONG, L.; GUO, J.; ZHU, A. Automated Extraction of Lake Water Bodies in Complex Geographical Environments by Fusing Sentinel-1/2 Data. **Water**, [S.l.], v. 14, n. 1, p. 30, 2021. <http://dx.doi.org/10.3390/w14010030>
- MARTINEZ, J; LETOAN, T. Mapping of flood dynamics and spatial distribution of vegetation in the Amazon floodplain using multitemporal SAR data. **Remote Sensing Of Environment**, [S.l.], v. 108, n. 3, p. 209-223, 2007. <http://dx.doi.org/10.1016/j.rse.2006.11.012>
- NASIR, N; KANSAL, A.; ALSHALTONE, O.; BARNEIH, F.; SHANABLEH, A.; AL-SHABI, M.; SHAMMAA, A. A. Deep learning detection of types of water-bodies using optical variables and ensembling. **Intelligent Systems With Applications**, [S.l.], v. 18, p. 200222, 2023. <http://dx.doi.org/10.1016/j.iswa.2023.200222>.
- PLANET, Analytic Imagery and Archive. 2023. Available: <https://www.planet.com/products/planet-imagery/>. Accessed on: nov. 10, 2023.
- PINHEIRO, M. M. F. **Aprendizagem profunda na segmentação semântica de rios em imagens de alta resolução espacial**. 2023. 102 f. Tese (Doutorado em Meio Ambiente e Desenvolvimento Regional) - Universidade do Oeste Paulista, Presidente Prudente, 2023.
- RAJENDIRAN, N.; KUMAR, L. S. Pixel Level Feature Extraction and Machine Learning Classification for Water Body Extraction. **Arabian Journal for Science and Engineering**, [S.l.], v. 48, n. 8, p. 9905-9928, 2022. <http://dx.doi.org/10.1007/s13369-022-07389-x>
- SALAH, M. A survey of modern classification techniques in remote sensing for improved image classification. **Journal of Geomatics**, v. 11, n. 1, 2017. Available: <http://isgindia.org/wp-content/uploads/2017/04/016.pdf>. Accessed on: mar. 27, 2023.
- SON, N.-T.; CHEN, C.-F.; CHEN, C.-R.; TOSCANO, P.; CHENG, Y.-S.; GUO, H.-Y.; SYU, C.-H. A phenological object-based

- approach for rice crop classification using time-series Sentinel-1 Synthetic Aperture Radar (SAR) data in Taiwan. **International Journal Of Remote Sensing**, [S.l.], v. 42, n. 7, p. 2722-2739, 2021. <http://dx.doi.org/10.1080/01431161.2020.1862440>
- TAMIRU, H.; DINKA, M. O. Application of ANN and HEC-RAS model for flood inundation mapping in lower Baro Akobo River Basin, Ethiopia. **Journal Of Hydrology: Regional Studies**, [S.L.], v. 36, p. 100855, ago. 2021. <http://dx.doi.org/10.1016/j.ejrh.2021.100855>.
- TIAN, Y.; CHEN, X.; LUO, P.; XU, Y. Beijiang water body information extraction based on ENVISAT-ASAR. 2012 **Second International Workshop On Earth Observation and Remote Sensing Applications**, [S.l.], v. 5, n. 8, p. 100-115, jun. 2012. <http://dx.doi.org/10.1109/eorsa.2012.6261181>
- WANG, X.; GE, L.; LI, X. Pasture Monitoring Using SAR with COSMO-SkyMed, ENVISAT ASAR, and ALOS PALSAR in Otway, Australia. **Remote Sensing**, [S.l.], v. 5, n. 7, p. 3611-3636, 2013. <http://dx.doi.org/10.3390/rs5073611>.
- XIE, Y.; CHEN, R.; YU, M.; RUI, X.; DU, X. Improvement and application of UNet network for avoiding the effect of urban dense high-rise buildings and other feature shadows on water body extraction. **International Journal Of Remote Sensing**, [S.l.], v. 44, n. 12, p. 3861-3891, 2023. <http://dx.doi.org/10.1080/01431161.2023.2229498>.
- ZHANG, Z.; ZHANG, X.; JIANG, X.; XIN, Q.; AO, Z.; ZUO, Q.; CHEN, L. Automated Surface Water Extraction Combining Sentinel-2 Imagery and OpenStreetMap Using Presence and Background Learning (PBL) Algorithm. **Ieee Journal of Selected Topics In Applied Earth Observations And Remote Sensing**, [S.l.], v. 12, n. 10, p. 3784-3798, 2019. <http://dx.doi.org/10.1109/jstars.2019.2936406>

AUTHOR CONTRIBUTION

Juarez Antônio da Silva Júnior conceptualized the work, carried out the methodology, analyzed the software, validated the data, and wrote and prepared the original draft. Ubiratan Joaquim da Silva Junior performed the formal analysis and visualized and curated data. The two authors investigated, wrote, reviewed and edited the text. Furthermore, the authors supervised and managed the project. All authors read and agreed to the published version of the manuscript.



This is an Open Access article distributed under the terms of the Creative Commons Attribution License, which permits unrestricted use, distribution, and reproduction in any medium, provided the original work is properly cited.